BMC Microbiology

RESEARCH

Open Access

Effects of USP25 knockout on the gut microbial diversity and composition in mice

Jinqiu Li[1†], Zhonghui Chen[1†], Xingchen Yan[2†], Qizhou Chen[3], Cirong Chen[3], Huan Liu[4*] and Jianlin Shen[1*]

Abstract

Background The gut microbiota plays a crucial role in host health. Recent study revealed that ubiquitin-specific protease 25 (USP25) deficiency affected colonic immune responses and resistance to certain bacterial infection. This study aimed to investigate the impact of USP25 gene deletion on the gut microbiota of mice, utilizing 16 S rRNA amplicon sequencing and metagenomic sequencing to provide a comprehensive analysis of microbial diversity, composition and functional characteristics.

Methods We collected fecal samples from 10 wild type (WT) C57BL/6J mice and 10 USP25$^{-/-}$ mice (C57BL/6J-Usp25^{em1}cyagen) for 16 S rRNA amplicon sequencing. Subsequently, the 6 of the 20 samples underwent further analysis using metagenomic sequencing.

Results Our results revealed significant differences in the gut microbiota between USP25 knockout (KO) mice and wild-type (WT) controls, with KO mice exhibiting 1,858 unique amplicon sequence variants (ASVs) compared to 1,723 in WT mice. Notably, the KO group displayed a higher tendency for biofilm formation and a greater proportion of gram-negative bacteria, while the WT group demonstrated enhanced stress tolerance and a higher presence of gram-positive bacteria. Functional prediction analyses indicated an increase in antibiotic resistance genes in the KO mice, particularly for tetracycline, cephalosporin, and sulfonamides, suggesting a potential risk for clinical antibiotic treatment efficacy. Moreover, KEGG pathway enrichment analysis revealed significant enrichment for fructose and mannose metabolism, streptomycin biosynthesis in the KO group. Furthermore, an increase in protective microbes alongside a decrease in potential pathogens in the KO microbiota hinted at altered immune responses due to USP25 deletion.

Conclusion Our findings elucidate the essential role of USP25 in modulating gut microbiota composition and function, providing insights for future therapeutic strategies targeting gut microbiota in disease contexts.

Clinical trail number Not applicable.

Keywords USP25, Gut microbiota, 16S rRNA sequencing, Metagenomic sequencing, Antibiotic resistance, Host-microbe interactions

†Jinqiu Li, Zhonghui Chen and Xingchen Yan contributed equally to this work as co-first authors.

*Correspondence:
Huan Liu
20016040@163.com
Jianlin Shen
shenjianlinchina@126.com

Full list of author information is available at the end of the article

Introduction

Ubiquitin-specific protease 25 (USP25) belongs to the ubiquitin-specific protease (USP) family, which plays a pivotal role in the regulation of ubiquitin-mediated protein degradation. The ubiquitin-proteasome system is crucial for maintaining cellular homeostasis by modulating the turnover of regulatory proteins involved in various cellular processes, such as cell cycle, apoptosis, signal transduction, and protein quality control [1]. USP25, in particular, has attracted considerable attention due to its emerging involvement in various diseases [2], including cancer [3], neurodegenerative disorders [4], and immune responses to viral infections [5].

Extensive studies have characterized the structural and functional attributes of USP25 [6], which is composed of multiple domains, including a ubiquitin-binding region (UBR) at the N-terminus, a ubiquitin-associated domain (UBA), a ubiquitin interacting motif (UIM), a small ubiquitin-like modification domain (SIM), a catalytic USP domain and a C-terminal crimped domain [7]. Interestingly, USP25 exhibits a unique autoinhibitory mechanism, wherein its homotetrameric structure, formed by the dimerization of dimers, results in the inhibition of its enzymatic activity [8]. This regulatory mechanism is crucial, as it ensures that the activity of USP25 is meticulously controlled within the cellular environment.

Research has elucidated the role of USP25 in antiviral immunity, as it modulates immune responses by deubiquitinating key signaling molecules such as TRAF3 and TRAF6, thus affecting the activation of transcription factors like IRF3 and NF-κB [9]. Furthermore, USP25 has been implicated in neurodegenerative diseases, including Alzheimer's disease [10], where it affects the stability of proteins involved in amyloid precursor protein processing and the inflammatory response [11]. Recently, USP25 has also been shown associated with bone mineral density in women [12].

In the area of cancer research, the role of USP25 is quite complex and multifaceted. USP25 has been found to be overexpressed in various cancer tissues, including breast [13], liver [14], pancreatic [15], and colorectal cancers [16], with elevated levels often correlated with poor prognosis. The mechanistic insights of USP25 in cancer biology are gradually being unraveled, with studies indicating its involvement in promoting tumor growth, metastasis, and resistance to therapy. For instance, USP25 has been shown to stabilize hypoxia-inducible factor-1 alpha (HIF-1α), a key regulator of the glycolytic pathway in pancreatic cancer, thereby promoting tumor growth and metabolic reprogramming [15].

Investigations utilizing USP25 gene knockout (KO) mice have yielded valuable insights into the physiological functions [15, 16]. These USP25 KO mice exhibit enhanced colonic immune responses and increased resistance to certain bacterial infection [16], thus may affect gut microbial diversity and composition. USP25 deficiency may exert an impact on the gut microbiota by altering the pathways within the host cells, such as STAT3 and Wnt signaling. However, most studies have focused on the direct cellular effects of USP25, with limited attention paid to its potential influence on the gut microbiota.

This study aims to fill this research gap by investigating the gut microbiota composition in USP25 KO mice through 16 S rRNA sequencing and metagenomic analysis. By comparing the fecal microbiota of USP25 KO mice with their wild-type counterparts, we aim to elucidate the impact of USP25 on the gut microbiome and its potential implications for host health and disease susceptibility.

Materials and methods

Gene knockout mice and sample collection

Wild type (WT) C57BL/6JCya mice and USP25$^{-/-}$ mice (C57BL/6JCya-Usp25^{em1}/cya, serial number: KOCMP-30940-Usp25-B6J-VA) were both generated by Cyagen Biosciences Inc.(Guangzhou, China). 10 WT mice and 10 USP25$^{-/-}$ mice were housed separately in a specific-pathogen-free animal facility with a 12-h dark/12-h light cycle and fed with water and irradiation sterilized food for laboratory mouse growth and reproduction (Xietong Bio Inc., Jiangsu, China). The environmental temperature and humidity were maintained at 20–26℃ and 40-70%, respectively. Sex and age details were indicated in Supplementary Table 1. Before fecal sampling, each mouse was individually and gently transferred to a separate, clean, and disinfected cage to prevent cross-contamination. Fecal pellets were collected from the bottom of the cage using a sterile disposable plastic spatula. Select fecal pellets that were intact and free of contamination. Immediately after collection, fecal samples were transferred into sterile tubes and then stored at -80℃ for subsequent analysis, ensuring the integrity of the microbiome.

After the animal experiment, all mice were systematically and humanely euthanized in groups using carbon dioxide (CO_2) asphyxiation. Briefly, mice were gently placed in a clean polyurethane box connected to a CO_2 tank, with a flow rate set at 30% of the chamber volume per minute. Mice remained in the chamber until they ceased respiratory movements for 2 min. They were then removed and cervically dislocated as a secondary method of euthanasia. All experimental protocols conducted in this study were approved by the Ethics Committee of the Affiliated Hospital of Putian University (approval number: PYFL202308).

DNA extraction and PCR amplification

Genomic DNA from a total of 20 samples was isolated utilizing the PF Mag-Bind Stool DNA Kit (Omega, USA),

following strictly to the manufacturer's guidelines. The assessment of DNA quality was performed through 1.0% agarose gel electrophoresis, and concentration was measured by a NanoDrop ND-2000 spectrophotometer (Thermo Scientific, USA). And the hypervariable region V3-V4 of bacterial 16 S rRNA gene was amplified using primer pairs 338 F (5'-ACTCCTACGGGAGGCAGCA G-3') and 806R (5'-GGACTACHVGGGTWTCTAAT-3') [17] by a GeneAmp 9700 PCR thermocycler (ABI, USA). The PCR mixture consisted of 4 μL of 5 × Fast Pfu buffer, 2 μL of dNTPs (2.5 mM), 0.8 μL of each primer (5 μM), 0.4 μL of Fast Pfu polymerase, 10 ng of template DNA, and distilled deionized water to achieve a final volume of 20 μL. The amplification procedure included initial denaturation at 95 ℃ for 3 min, followed by 27 cycles comprising denaturation at 95 ℃ for 30 s, annealing at 55 ℃ for 30 s, and extension at 72 ℃ for 45 s, concluding with a single extension step at 72 ℃ for 10 min, and finishing at 4 ℃. All samples underwent amplification in triplicate. These PCR products were extracted from a 2% agarose gel and subsequently purified, followed by quantification with a Quantus Fluorometer (Promega, USA).

Illumina sequencing

Purified amplicons were combined in equal molar concentrations and subjected to paired-end sequencing using the Illumina Novaseq PE250 platform (Illumina, USA), following the standard procedures established by Majorbio Bio-Pharm Technology Co. (Shanghai, China). For metagenomic sequencing, six chosen DNA extracts underwent fragmentation to achieve an average length of approximately 400 base pairs, utilizing the Covaris M220 system (Gene Co. Ltd., China). Subsequently, a paired-end library was generated employing the Nextflex Rapid DNA-Seq kit (Bio Scientific, USA). The actual metagenomic sequencing was conducted on the Illumina Novaseq 6000 platform (Illumina, USA), utilizing the NovaSeq 6000 S4 Reagent Kit in accordance with the protocols. Both sequencing data generated from this study have been deposited in the NCBI Short Read Archive (SRA) database (accession number: PRJNA1149551).

Amplicon sequence processing and analysis

After demultiplexing, the resulting sequences were quality-filtered with fastp (0.19.6) [18] and merged with FLASH (v1.2.11) [19] with the following criteria: (1) the reads were truncated at any site receiving an average quality score of < 20 over a 50-base pairs (bps) sliding window, and the truncated reads shorter than 50 bps were discarded, reads containing ambiguous characters were also discarded; (2) only overlapping sequences longer than 10 bps were assembled according to their overlapped sequence. The maximum mismatch ratio of overlap region is 0.2. Reads that could not be assembled were discarded; (3) samples were distinguished according to the barcode and primers, and the sequence direction was adjusted, exact barcode matching, 2 nucleotide mismatch in primer matching.

Then the high-quality sequences were de-noised using the DADA2 [20] plugin in the QIIME2 [21](version 2020.2) pipeline with recommended parameters, which obtains single nucleotide resolution based on error profiles within samples. DADA2-denoised sequences are usually called amplicon sequence variants (ASVs). Taxonomic assignment of ASVs was performed using the Naive Bayes consensus taxonomy classifier implemented in QIIME2 and the SILVA 16 S rRNA database (v138). The metagenomic function was predicted by PICRUSt2 [22] based on ASV representative sequences. PICRUSt2 is a software containing a series of tools as follows: HMMER was used to align ASV representative sequences with reference sequences. EPANG and Gappa were used to put ASV representative sequences into a reference tree. The castor was used to normalize the 16 S gene copies. MinPath was used to predict gene family profiles and locate the gene pathways. The entire analysis process was according to the protocols of PICRUSt2. Functional prediction analysis of the mouse gut microbiota was conducted based on the BugBase phenotype database [23].

Bioinformatic analysis of 16 S rRNA sequencing

Bioinformatic analysis of the gut microbiota was conducted using the Majorbio Cloud platform (https://cloud.majorbio.com). Utilizing Mothur (v1.30.2), ASV data was used to calculate rarefaction curves and alpha diversity metrics, including observed ASVs, ACE, Chao, Shannon index, Simpson index and Good's coverage [24]. The similarity among the microbial communities across different samples was evaluated through principal coordinate analysis (PCoA) and PERMANOVA based on Bray-Curtis dissimilarity, using Vegan v2.4.3 package. The linear discriminant analysis (LDA) effect size (LEfSe) [25] was performed to identify the significantly abundant taxa (phylum to genera) of bacteria among the different groups (LDA score > 3, $P < 0.05$). Since there is a multicollinearity problem among the clinical parameters, the variance inflation factor (VIF) for each variable was estimated using the car package (https://cran.r-project.org/web/packages/car/car.pdf). The distanc e-based redundancy analysis (db-RDA) was performed using Vegan v2.4.3 to investigate the effect of clinical parameters on gut bacterial community structure. Linear regression analysis was applied to determine the association between major clinical parameters identified by db-RDA analysis and microbial alpha diversity indices. The co-occurrence networks were constructed to explore the internal community relationships across the samples [26]. A correlation between two nodes was considered to

be statistically robust if the Spearman's correlation coefficient was over 0.6 or less than – 0.6, and the P-value was less than 0.05.

Processing of metagenome sequencing data

The metagenomic data were also analyzed on the online platform (Majorbio Cloud Platform). Briefly, the raw sequencing reads were trimmed of adaptors, and low-quality reads (length < 50 bps or with a quality value < 20 or having N bases) were removed by fastp (https://github.com/OpenGene/fastp, version 0.20.0). Reads were aligned to the murine genome (GCA_000001635.9) by BWA [27] (http://bio-bwa.sourceforge.net, version 0.7.17) and any hit associated with the reads and their mated reads were removed. The quality-filtered data were assembled using MEGAHIT [28] (https://github.com/voutcn/megahit, version 1.1.2). Contigs with a length ≥ 300 bps were selected as the final assembling result. Open reading frames (ORFs) from each assembled contigs were predicted using Prodigal v2.6.3 (https://github.com/hyattpd/Prodigal) and a length ≥ 100 bps ORFs were retrieved. A non-redundant gene catalog was constructed using CD-HIT [29] (http://weizhongli-lab.org/cd-hit/, version 4.7) with 90% sequence identity and 90% coverage. Gene abundance for a certain sample was estimated by SOAPaligner [30] (https://github.com/ShujiaHuang/SOAPaligner, version soap 2.21) with 95% identity.

Taxonomic and functional annotation

The best-hit taxonomy of non-redundant genes was obtained by aligning them against the NCBI NR database by DIAMOND [31] (http://ab.inf.uni-tuebingen.de/software/diamond/, version 2.0.11) with an e-value cutoff of 1e-5. Similarly, the functional annotation (GO, KEGG, eggNOG, ARDB, CARD, PHI) of non-redundant genes was obtained. Based on the taxonomic and functional annotation and the abundance profile of non-redundant genes, the differential analysis was carried out at each taxonomic, functional, or gene-wise level by the Kruskal-Wallis test.

Results

16S rRNA amplicon sequencing data summary

In this study, 16S rRNA amplicon sequencing was applied to reveal the differences in the gut microbiome between USP25 knockout (KO) mice ($n = 10$) and wild-type (WT) mice ($n = 10$). To show that USP25 is not expressed in the KO mice, RNA was extracted from the blood of both KO and WT mice and quantitative PCR was performed using specific USP25 primers. We detected the expression of USP25 mRNA in WT mice, while USP25 mRNA was not detected in KO mice (Data not shown).

A total of 709,142,222 bps and 1,679,292 sequences were obtained from the raw data, with an average of 83,965 ± 9,334 sequences per sample and an average of 422.4 ± 2.4 bps per sequence (Supplementary Table 2). All sequences were then processed by DADA2 and the denoised sequences were usually called amplicon sequence variants (ASVs). After processing, a total of 720,935 clean sequences and 8,122 ASVs were obtained, and the average ASV numbers obtained from USP25 KO (427.9 ± 39.4) and WT (384.3 ± 73.3) mice were not significantly different (Supplementary Table 2). KO and WT mice shared 224 common ASVs, with 1,858 and 1,723 unique ASVs, respectively.

To explore the microbial diversity in these two groups, we then analyzed Chao, coverage, Shannon, Simpson, ACE, and Sobs, as the six common alpha diversity indexes of the gut microbe. All six indexes showed no significant difference in microbiota diversity between the USP25-KO and WT mice (Fig. 1A and Supplementary Fig. 1). Though the Wilcoxon rank-sum test of beta diversity analysis showed no significant difference ($P > 0.05$, Fig. 1B), hierarchical clustering analysis (ASV level) using the Bray-Curtis dissimilarity metric demonstrated distinct clustering patterns between the USP25-KO and WT groups (Fig. 1C). And heatmap of dissimilarity between samples also revealed the differences between these two groups (Fig. 1D). Principal coordinates analysis (PCoA) using Bray-Curtis distances generated from relative abundances of ASV level was performed. The first principal axis (PC1) could explain 36.38% of the sample differences, and the second principal axis (PC2) could explain 14.82% of the sample differences (Fig. 1E). The PCoA plot showed a clear separation between the microbial profiles of the USP25-KO and WT groups on the PC1-axis. Furthermore, Principal component analysis (PCA) and non-metric multidimensional scaling analysis (NMDS) were performed and confirmed the significant differences (Supplementary Fig. 1). These findings indicate that a lack of USP25 alters gut microbial diversity in adult mice.

Taxonomic composition of the gut microbiota in USP25 KO and WT mice

Briefly, USP25 KO and WT mice shared common 14 phyla, 111 genera, and 224 ASVs (Fig. 2A). Compared with the WT group had unique 3 phyla, 50 genera, and 1,723 ASVs, the KO group especially possesses 3 phyla, 64 genera, and 1,858 ASVs. Circos plot indicated the relative composition distribution of gut microbiota between individual samples and specific phyla. The top 5 dominant phyla of the two groups were *Fimicutes*, *Bacteroidota*, *Verrucomicrobiota*, *Actinobacteriota*, and *Campilobacterota* (Fig. 2B). Individual taxonomic composition of the gut microbiota at the genus level were shown in Fig. 2C, *Lactobacillus*, *norank_f_Muribaculaceae*, *unclassified_f_Lachnospiraceae*, *Bacteroides*, and *Alistipes* were the top 5 dominant genera in the two groups.

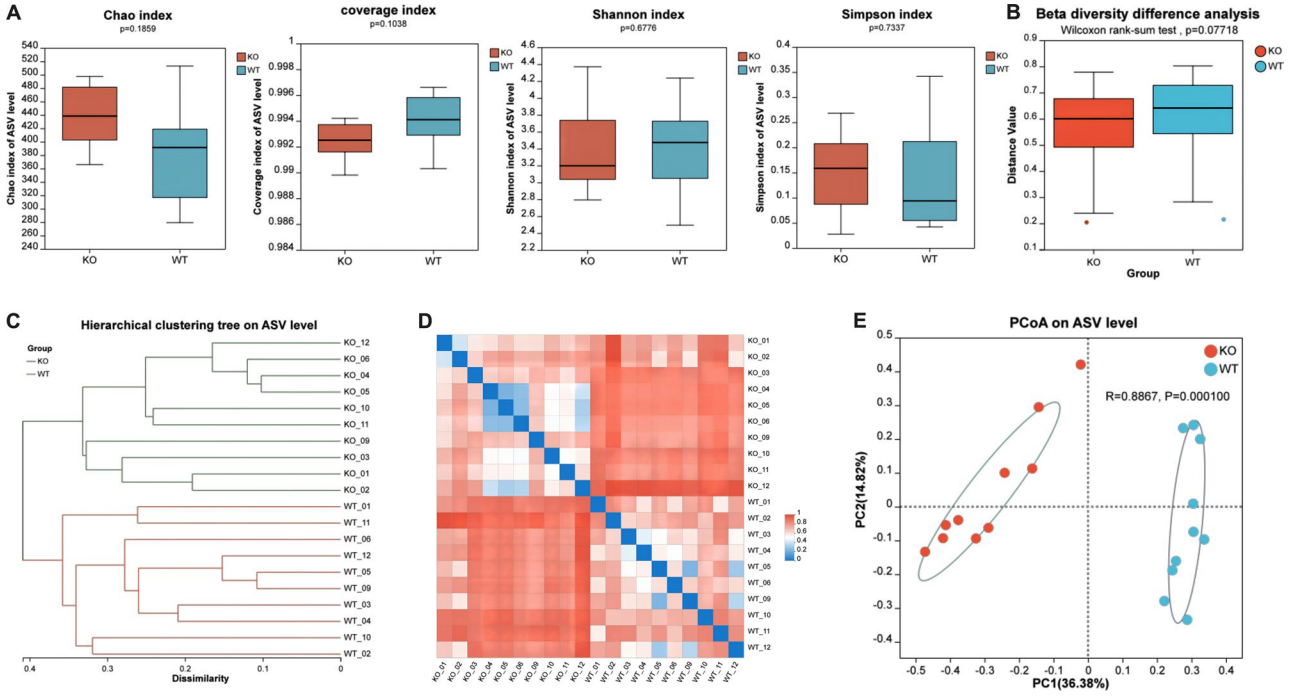

Fig. 1 Alpha and Beta diversity of the gut microbiota in the USP25 KO and WT mice. (**A**) Boxplot illustrating comparisons of 4 alpha diversity indexes (Chao, coverage, Shannon, and Simpson) between groups. Wilcoxon rank-sum test, $n = 10$. (**B**) Beta diversity difference analysis of these two groups. Wilcoxon rank-sum test, $n = 10$. (**C**) Hierarchical clustering trees of samples on ASV level based on the Bray-Curtis method. (**D**) Heatmap of distance relationship between samples. The dissimilarity values were normalized to a range from 0 to 1. (**E**) Principal coordinate analysis (PCoA) of the gut microbiota using the Bray-Curtis distance metric. Each point represents the composition of the fecal microbiota of one sample

The gut microbiota difference between USP25 KO and WT mice

To further determine the effect of USP25 deficiency on the specific gut microbial communities, a Wilcoxon rank-sum test and a Linear discriminant (LDA) and effect size (LEfSe) analysis were performed to discover the different biomarkers in the microbiomes between groups (Fig. 3). At the genus level, *norank_f_Muribaculaceae*, *Bacteroides*, *Alloprevotella*, *Prevotellaceae_UCG-001*, *norank_Oscillospiraceae*, and *unclassified_f_Oscilospiraceae* were enriched significantly in the WT mice, whereas *Alistipes*, *Lachnospiraceae_NK4A136_group*, *Odoribacter*, and *Enterorhabdus* were enriched significantly in USP25-KO group (Fig. 3A). At the class level, *Coriobacteriia*, and *Deferribacteres* were enriched in USP25-KO mice, whereas *Bacteroidia*, *Gemmatimonadetes*, and *Vampirivibrionia* were enriched in the WT mice (Fig. 3B-C). At the order level, *Coriobacteriales*, *Flavobacteriales*, *Rhizobiales*, *Clostridiales*, and *Deferribacterales* were enriched in the KO mice, while *Bacteroidales*, *Oscillospirales*, *Gemmatimonadales*, *Gastranaerophilales*, and *Rhodospirillales* were enriched in the WT mice (Fig. 3B-C). At the family level, *Rikenellaceae*, *Marinifilaceae*, *Butyricicoccaceae*, *Flavobacteriaceae*, *Clostridiaceae*, *Deferribacteraceae*, *Streptococcaceae*, *Eggerthellaceae*, and *Atopobiaceae* were enriched in the KO mice, while *Muribaculaceae*, *Prevotellaceae*, *Bacteroidaceae*, *Oscillospiraceae*, *Erysipelatoclostridiaceae*, *Gemmatimonadaceae*, *Acholeplasmataceae*, and *Tannerellaceae* were enriched in the WT mice (Fig. 3B-C). 60 important taxonomic differences between the two groups were indicated in Fig. 3C. Taken together, these results suggest that systemic USP25 deletion alters the enrichment of the specific gut bacteria in mice.

Phenotype prediction of mice based on 16 S rRNA sequencing

Functional prediction analysis of the mouse gut microbiota was conducted based on the BugBase phenotype database. As shown in Fig. 4A, the significant differences in phenotype between these two groups were forms biofilms, facultatively anaerobic, gram-negative, gram-positive, and stress tolerant. In USP25-KO mice, the microbial communities predominantly exhibit gram-negative and demonstrate a propensity for biofilm formation. Conversely, the WT group is inclined to harbor gram-positive bacteria that are more facultatively anaerobic and possess enhanced stress tolerance. Contributions of different gut microbiota at the genus level were described by stacked bar chart in Fig. 4B-F. Increased abundance of *Erysipelatoclostridium*, *Candidatus Stoquefichus*, and *unclassified_f_Erysipelotrichaceae* made the WT group more facultatively anaerobic (Fig. 4B). *Enterorhabdus* and *Parvibacter* were the dominant microbes in KO mice in

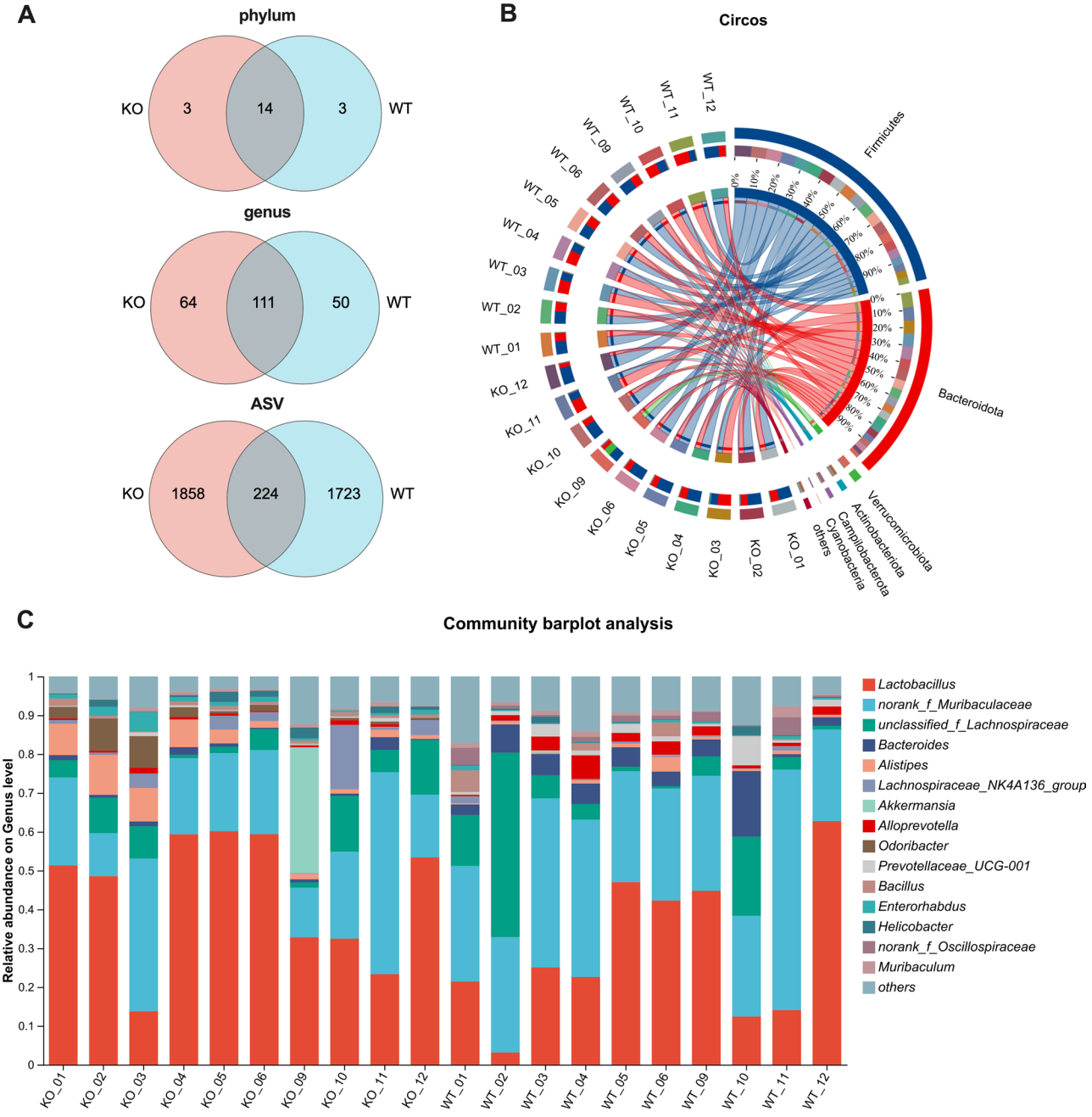

Fig. 2 Taxonomic composition of gut microbiota between USP25 KO and WT mice. (**A**) Venn plot showed the specific and common numbers in gut microbiota at the phylum, genus, and ASV levels. (**B**) Circos plot indicated the composition distribution of individual samples at the phylum level. Six top dominant phyla were shown in the right part. (**C**) Composition bars of the gut microbiota at the genus level. 15 top genera were shown in different colors

forming biofilms (Fig. 4C). *Norank_f_Muribaculaceae*, *Helicobacter*, *Alistipes*, and *Odoribacter* contribute to gram-negative in the USP25 KO group, while *Lactobacillus* and *norank_f_Ruminococcaceae* in the WT group showed gram-positive (Fig. 4D-E). Reduce of *Lactobacillus* and gain of *Alistipes* lead to less stress tolerance in the microbial communities of USP25 KO mice (Fig. 4F).

Taxonomic composition and difference based on metagenomic sequencing

Metagenomic sequencing data showed that USP25-KO and WT mice shared common 109 phyla, 1,452 genera, and 5,222 species (Fig. 5A). Compared with the WT group, the KO group especially possesses 16 phyla, 397 genera, and 1,992 species. Figure 5B presents the detailed composition of the gut microbiota of individual samples at the genus level.

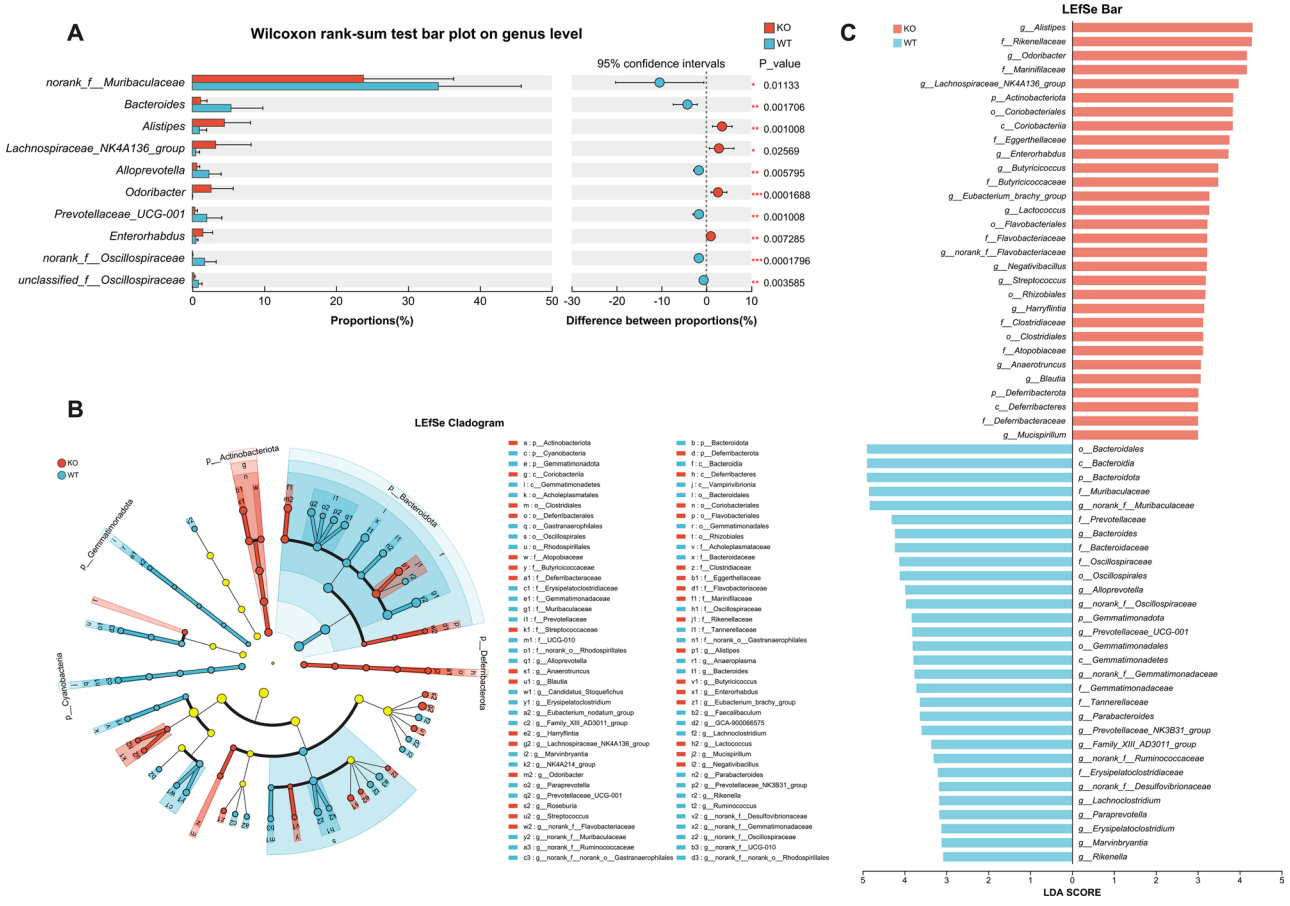

Fig. 3 LEfSe analysis of gut microbiota between USP25 KO and WT mice. (**A**) The bar plot showed 10 top genera with significant differences ($P < 0.05$) between the two groups. Comparisons were conducted using a Wilcoxon rank sum test. A red asterisk indicated the significant difference ($P < 0.05$). (**B**) The LEfSe cladogram of taxonomic differences in the gut microbiota between these two groups. (**C**) The LEfSe bar plot represents the significantly differential taxa between USP25 KO (red) and WT (blue) mice, based on effect size (LDA Score > 3)

Bacteroides, *unclassified_f_Lachnospiraceae*, *Prevotella*, *Ligilactobacillus*, *Muribaculum*, *Duncaniella*, *Alistipes*, *unclassified_f_Muribaculaceae*, *Barnesiella*, and *Lactobacillus* were the 10 dominant genera in the gut microbiota of both groups (Fig. 5B). *Bacteroides*, *Ligilactobacillus*, *Parabacteroides*, *unclassified_f_Bacteroidaceae*, *Erysipelatoclostridium*, and *Muribaculum* reduced significantly ($P < 0.05$) in USP25 deficient mice (Fig. 5C).

To explore the functional potential of the gut microbiota and to find some specific metabolic pathways, a KEGG pathway enrichment analysis was conducted. As was shown by the Venn plot in Fig. 6A, USP25-KO and WT mice shared 381 common KEGG pathways, while KO and WT respectively possess 8 and 22 unique pathways. The top 10 pathways of significant difference between the two groups were fructose and mannose metabolism, streptomycin biosynthesis, other glycan degradation, propanoate metabolism, inositol phosphate metabolism, degradation of aromatic compounds, acarbose and validamycin biosynthesis, meiosis-yeast, naphthalene degradation, and retinol metabolism (Fig. 6B). And 25 most enriched KEGG pathways in either KO or WT groups were shown in Fig. 6C.

Function analysis of metagenomic data

The metagenomic analysis of the microbiome samples revealed a significant presence of antibiotic-resistance genes, as elucidated by the ARDB and CARD databases. The results indicated a substantial variation in the proportions of resistance genes between the KO and WT samples, with several genes showing statistically significant differences ($P < 0.05$), denoted by asterisks in Fig. 7. The top 3 antibiotic types with significant differences were tetracycline, cephalosporin, and sulfonamide (Fig. 7A). Notably, the genes *ZP_03923764* and *ZP_002236533* exhibited higher proportions in the KO group compared to the WT (Fig. 7B). Conversely, the other 8 genes *ZP_03958019*, *ZP_03284557*, *ZP_02068298*, *YP_001969930*, *BAD65785*, *ZP_04623431*, *AAD23513*, and *ZP_03013260* were found in lower proportions in the KO samples. The genes *optrA*, *lmrD*, *tetB(P)*, *tetT*, and *lmrC* were higher in the WT group

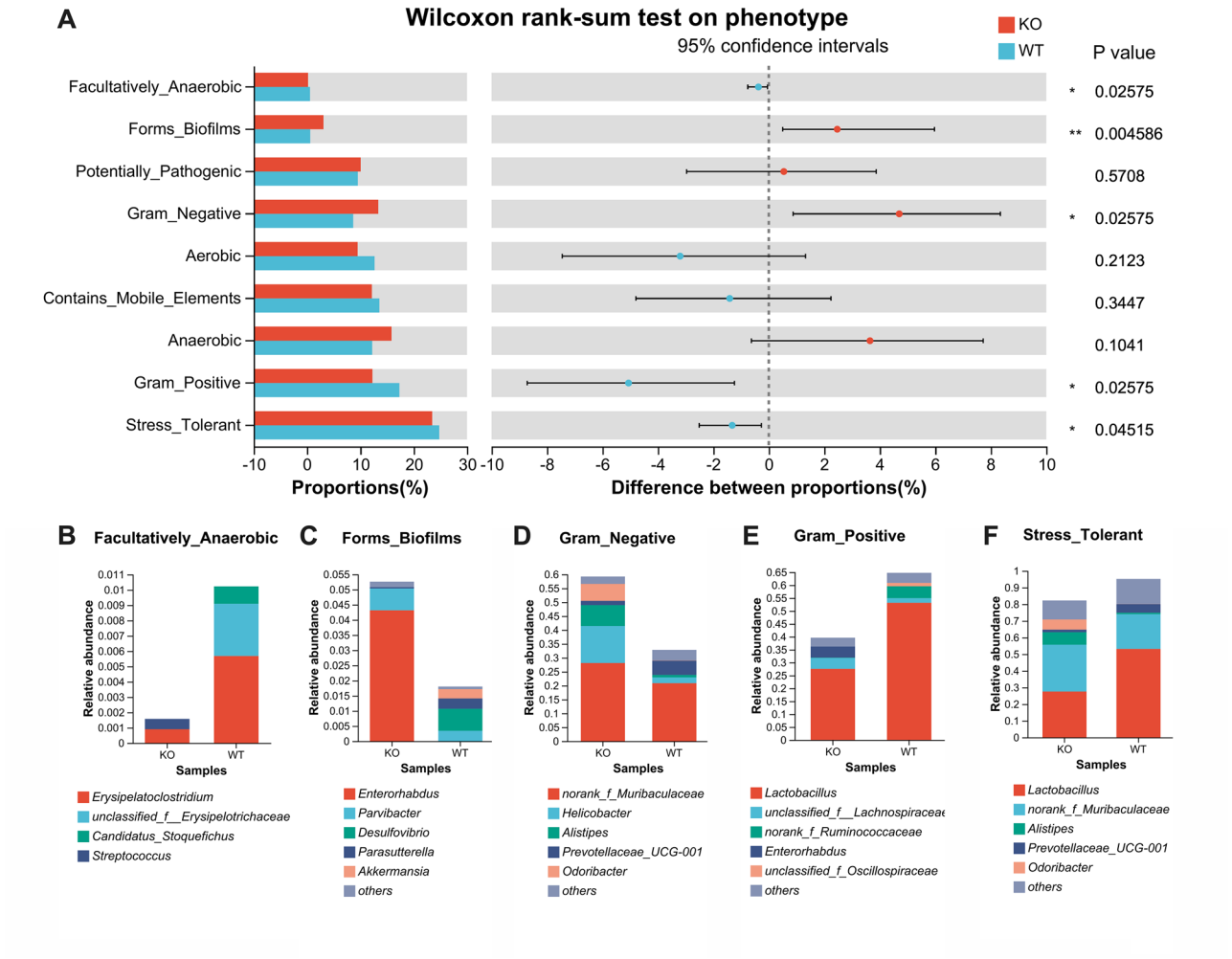

Fig. 4 Functional prediction analysis of the mouse gut microbiota based on the BugBase phenotype database. (**A**) Wilcoxon rank-sum test on phenotype. A asterisk indicated the significant difference ($P < 0.05$). (**B**-**F**) Contribution bars of gut microbiota to phenotype. Colors indicated different genera

while *vanSA*, *vanSM*, *vanSE*, *cfr(B)*, and *smeR* showed higher proportions in the KO mice (Fig. 7C).

In the probiotic category, the KO samples showed higher proportions of beneficial microbes such as *Clostridium* species, *Bacillus* species and *Faecalibacterium prausnitzii*, and possessed lower proportions of *Lactobacillus murinus* and *Lactobacillus* species, with P-values indicating significant differences compared to their WT counterparts (Fig. 8A). The pathogen species analysis indicated a reduced proportion of potential human pathogens such as *Enterococcus faecalis*, *Francisella tularensis* and *Actinobacillus pleuropneumoniae*, and a possible increase of *Enterococcus faecium* and *Vibrio vulnificus* in the USP25 deficient samples (Fig. 8B). Furthermore, the virulence factors analysis based on VFDB database (Fig. 8C) depicted a notable increase in the presence of various virulence factors (VFs) in the KO samples, including alginate (VF0091), polar flagella (CVF786), LPS (VF0033) and heme biosynthesis (CVF506), with decreased VFs such as capsule (VF0003), cytolysin (VF0356), colibactin (VF0573), Esp (VF0353), LPS (VF0171), and pyoverdine (CVF551) ($P < 0.05$). These changes indicated a complex pathogenic potential due to the USP25 deficiency.

Discussion

In the present study, utilizing advanced sequencing techniques, including 16 S rRNA amplicon sequencing and metagenomic analysis, we investigated the effects of USP25 gene deletion on the gut microbiome in mice, with a particular focus on its implications for microbial diversity and composition. Overall, the knockout of USP25 appears to have little impact on the alpha or beta diversity of the gut microbiota. Indexes of alpha diversity, which measure community richness (Sobs, Chao, and ACE) and evenness (Shannon, Simpson), show no significant differences between the KO and WT mice (Fig. 1 and Supplementary Fig. 1). This suggests that while USP25 may play

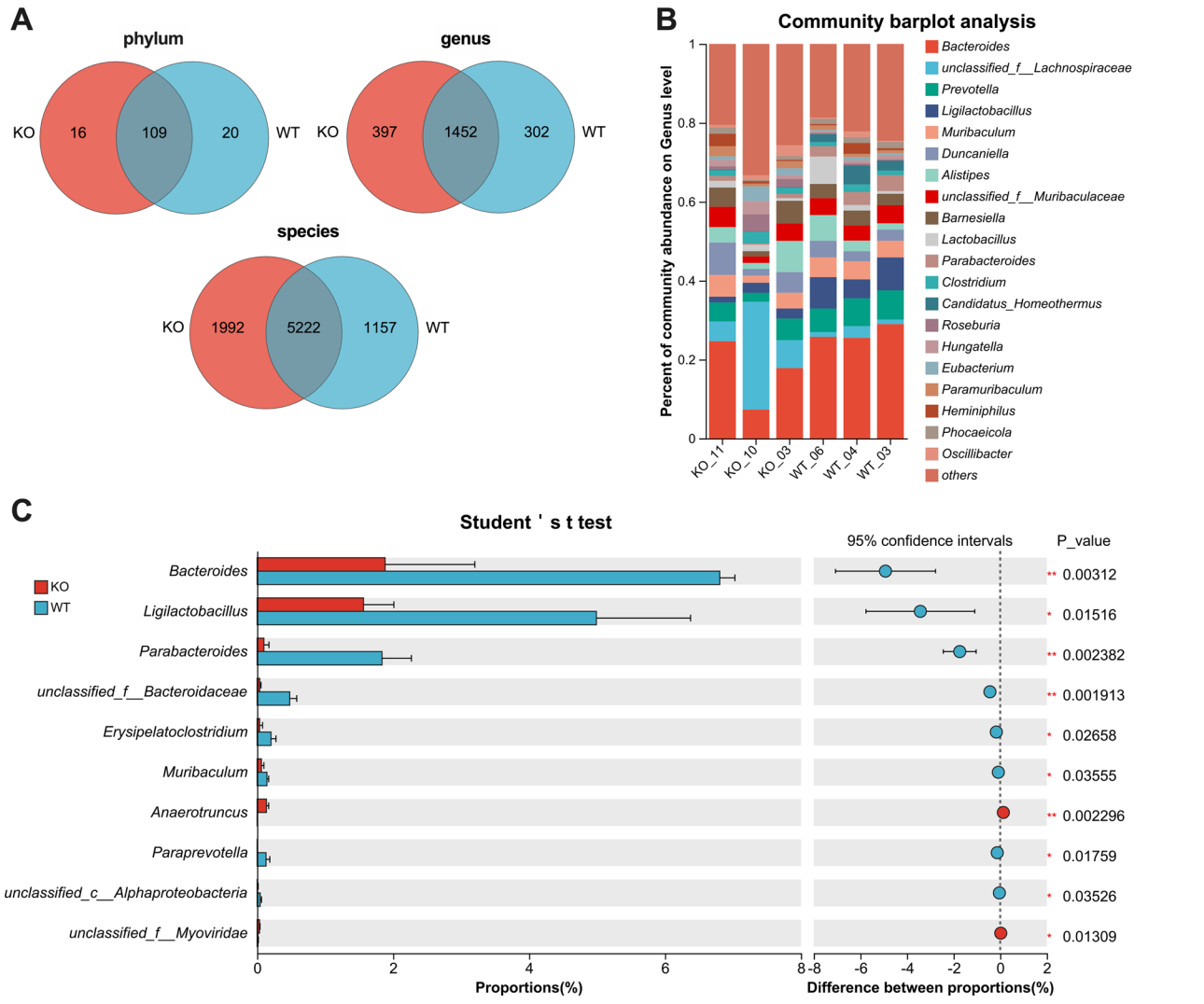

Fig. 5 Taxonomic comparison of gut microbiota in USP25-KO and WT mice. (**A**) Venn plot showed the unique and common numbers in gut microbiota at the phylum genus or species levels, respectively. (**B**) Taxonomic composition of the gut microbiota of individual samples at the genus level. Components of 20 top abundance were shown and residuals were combined into "others". (**C**) Bar plots of top 10 genera with significant differences between KO and WT mice. Wilcoxon rank-sum test. A red asterisk indicated the significant difference ($P < 0.05$)

a role in shaping the gut microbiota, its influence is not substantial. However, the distinct microbial composition observed between the two groups underscores the potential functional consequences of USP25 deficiency on the gut microbiota.

The Circos plot in Fig. 2B illustrated the dominant phyla of the gut microbiota in both groups, primarily composed of *Firmicutes*, *Bacteroidota*, *Verrucomicrobiota*, *Actinobacteriota*, and *Campilobacterota*. This composition aligns with previous studies, underscoring the prevalence of these phyla in gut microbial communities [32]. While 16 S rRNA sequencing and metagenomic sequencing revealed distinct microbial communities between groups, several genera exhibited high abundance rankings in both analyses. These included *Bacteroides*, *unclassified_f_Lachnospiraceae*, *Prevotellaceae*, *Muribaculum*, *Alistipes*, *Lactobacillus*, and *norank_f__Muribaculaceae*. Notably, metagenomic analysis showed that the abundance of *Bacteroides*, *Ligilactobacillus*, *Parabacteroides*, *Erysipelatoclostridium*, and *Muribaculum* was significantly reduced in the KO group compared to the WT group. This may highlight the complementary nature of the two sequencing methods in uncovering differential microbial profiles.

In this study, we observed that metagenomic sequencing offers a more comprehensive view of microbial communities (2,151 genera in total) compared to 16 S rRNA amplicon sequencing (225 genera in total), which

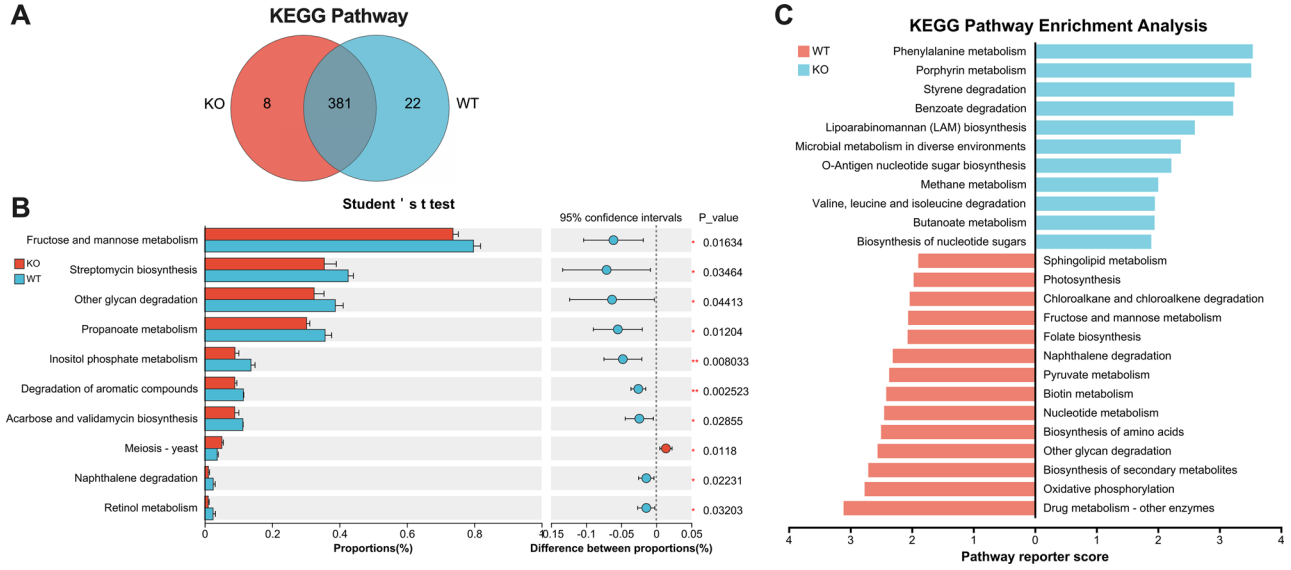

Fig. 6 KEGG pathway difference and enrichment analysis of metagenomic data in USP25-KO and WT mice. (**A**) Venn plot indicated numbers of the unique and common KEGG pathways in and between groups. USP25-KO (red), WT (blue). (**B**) Bar plots showed names of KEGG pathways with significant differences between groups. Student's t-test. A red asterisk indicated the significant difference ($P < 0.05$). (**C**) KEGG pathways enrichment analysis in USP25-KO and WT mice. Wilcoxon rank-sum test was conducted. USP25-KO (blue), WT (red)

primarily focuses on bacterial identification. Despite the similarities in findings between 16 S rRNA and metagenomic sequencing, discrepancies in community abundance were noted. For instance, the abundance of certain genera, such as *Bacteroides*, *Muribaculum*, *Alistipes*, and *Lactobacillus*, varied between the two sequencing methods. These differences may stem from the inherent limitations of each technique [33]. 16 S rRNA sequencing might introduce biases due to unequal amplification of species' 16 S rRNA genes, while metagenomic sequencing could lack sufficient depth to detect the 16 S rRNA genes of rare species within the community [34]. Moreover, the application of PICRUSt2 for functional prediction of 16 S rRNA gene data is subject to certain limitations, primarily due to its reliance on existing reference genome databases and the inherent assumptions regarding phylogenetic relationships [35]. The finite scope of these databases inevitably constrains the accuracy and comprehensiveness of functional annotations. Additionally, the complexity of phylogenetic relationships means that significant functional variations can occur even among microorganisms that are closely related phylogenetically [36]. These factors highlight the importance of considering the specific strengths and limitations of each sequencing method when interpreting microbial community data.

Phenotype prediction based on Bugbase indicates a propensity for biofilm formation and an increased abundance of gram-negative bacteria in USP25 KO mice, whereas WT mice exhibit a greater representation of facultatively anaerobic, gram-positive bacteria and enhanced stress tolerance. This observation implies that USP25 may influence microbial survival strategies and community structure. The capacity of certain bacterial species to form biofilms is known to impact their resilience within the gut environment and contribute to pathogenesis in various conditions, including inflammatory bowel disease [37]. Furthermore, the stress tolerance predicted in the WT microbiota raises concerns about the ecological stability of the KO microbiome and its implications for disease susceptibility. Investigating the mechanisms underlying these behavioral shifts may yield valuable insights into the role of USP25 in microbiome-host interactions and the potential for clinical applications targeting microbial behavior to enhance gut health [38].

The functional predictions indicating an increase in antibiotic resistance genes within the gut microbiota of USP25 KO mice present a concerning trend with potential clinical implications. The heightened prevalence of resistance genes against tetracycline, cephalosporin, and sulfonamides suggests that USP25 may play a critical role in regulating microbial resistance mechanisms [39, 40]. This finding aligns with emerging evidence linking genetic factors to the emergence and spread of antibiotic resistance within microbial communities. Consequently, further research is necessary to elucidate the pathways through which USP25 modulates resistance gene dynamics and to explore potential interventions that could restore microbial balance and enhance antibiotic efficacy.

In addition to the aforementioned observations, this study also has several limitations. For instance, the lack of

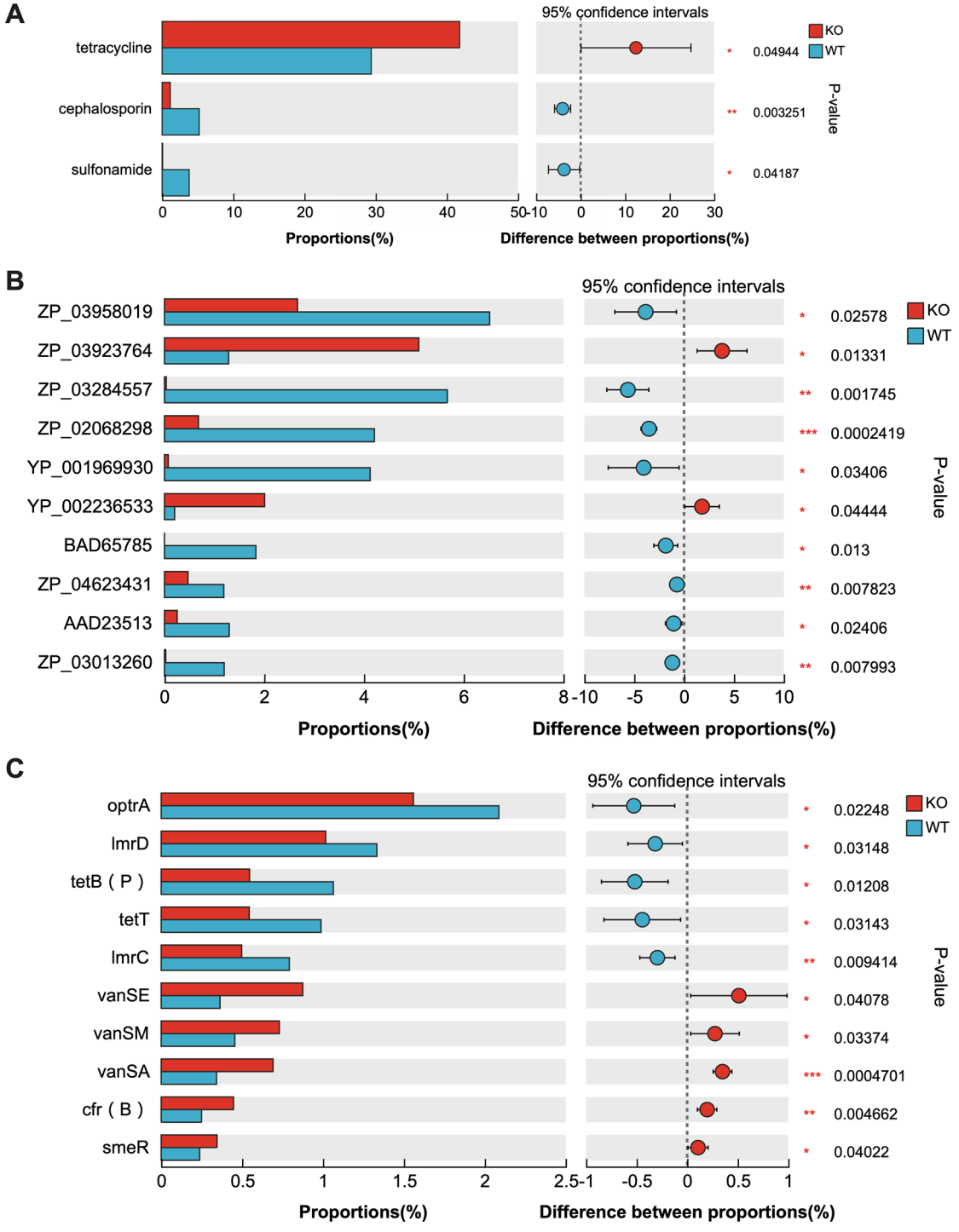

Fig. 7 Antibiotic prediction of metagenomic data based on ARDB and CARD databases. (**A**) Differences in the antibiotic type of ARDB between KO and WT groups. (**B**) Differences in antibiotic resistance genes (ARG) from ARDB between the two groups. (**C**) Differences in antibiotic resistance ontology (ARO) names in the CARD database between the two groups. Student's t-test. USP25-KO (red), WT (blue). A red asterisk indicated the significant difference ($P < 0.05$)

molecular pathway analysis in host cells limits our understanding of how changes in physiological and immune functions in mice following USP25 deficiency impact the composition and function of the gut microbiota. Furthermore, the absence of metabolite (or metabolome) measurements precludes us from identifying which molecules or metabolites such as short chain fatty acids, lipopolysaccharides and peptidoglycan are altered after

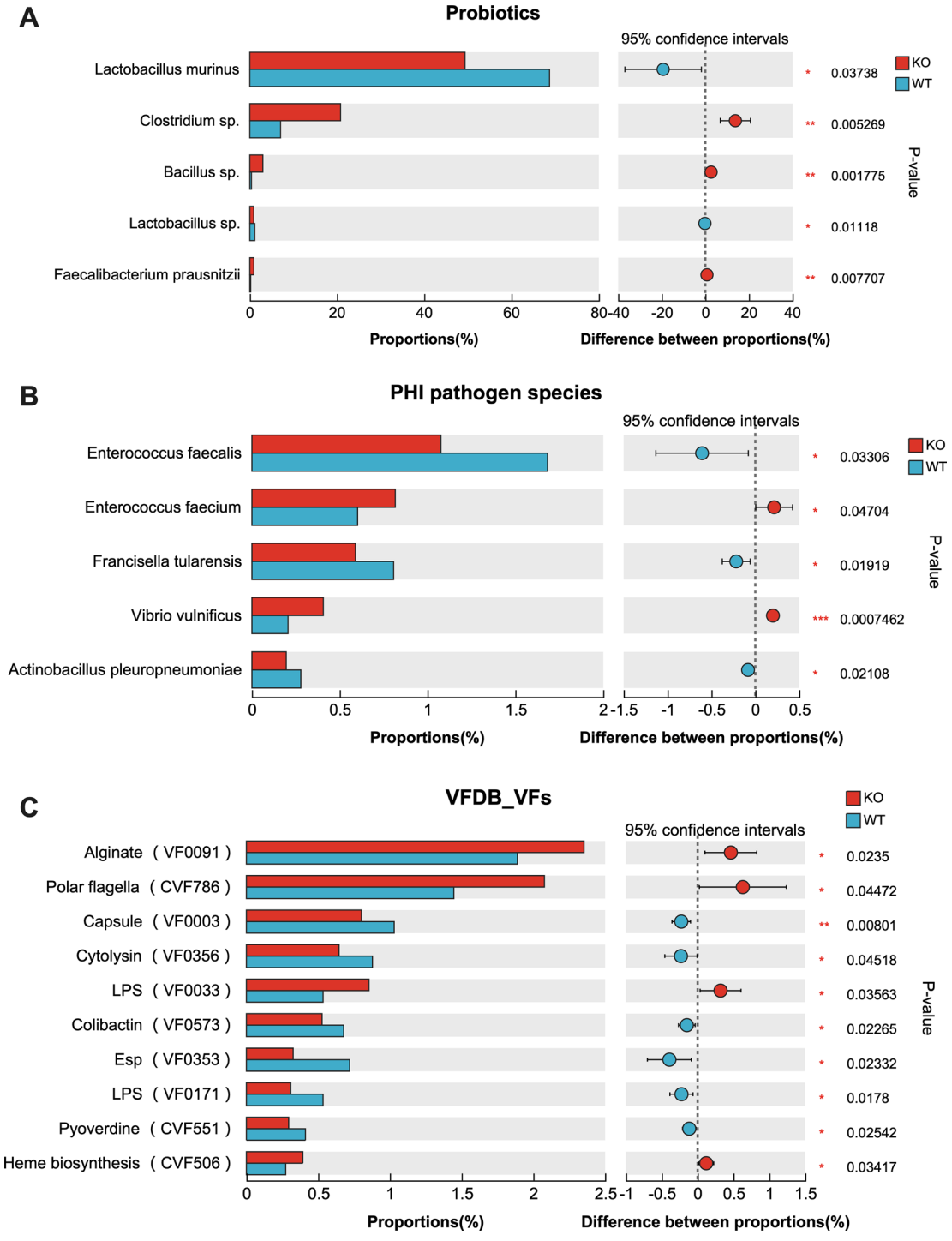

Fig. 8 (**A**) Top 5 probiotics with significant differences between groups. (**B**) PHI pathogen species and (**C**) Top 10 virulence factors (VFs) from the VFDB database. Student's t-test. USP25-KO (red), WT (blue). A red asterisk indicated the significant difference ($P < 0.05$)

USP25 deficiency and how these changes influence the regulation of intestinal cell states by microorganisms, thereby affecting host health [41]. Future research should focus on integrating multi-omics approaches, including metabolomics and transcriptomics, to provide a more comprehensive understanding of the interplay between USP25, gut microbiota, and host health.

Supplementary Information

The online version contains supplementary material available at https://doi.org/10.1186/s12866-025-04035-y.

Supplementary Material 1

Supplementary Material 2

Supplementary Material 3: Boxplot illustrating comparisons of 2 alpha diversity indexes ACE (A) and observed ASVs (Sobs) (B) between groups. n=10. Principal component analysis (PCA) (C) and non-metric multidimensional scaling (NMDS) (D) of the gut microbiota using the Bray-Curtis distance metric.

Author contributions
JL, ZC and XY conducted experiments and wrote the manuscript. QC and CC analyzed the data. JS and HL designed the experiments and revised the manuscript. JS, JL and HL acquired the funding. All the authors contributed to the article and approved the final manuscript.

Funding
This study was supported by the Natural Science Foundation of China (82301785), the Natural Science Foundation of Fujian Province (2022J011443, 2024J011450), and the Medical Research Foundation of Putian University (2024104, 2024112).

Data availability
All sequencing data have been uploaded to NCBI Short Read Archive (SRA) database (accession number: PRJNA1149551; web link: https://www.ncbi.nlm.nih.gov/bioproject/PRJNA1149551).

Declarations

Ethics approval and consent to participate
The experimental protocols conducted in this study were approved by the Ethics Committee of the Affiliated Hospital of Putian University (approval number: PYFL202308) and were performed following the Guidelines for Experimental Animals set by the Ministry of Science and Technology (Beijing, China).

Consent for publication
Not applicable.

Competing interests
The authors declare no competing interests.

Author details
[1]Central Laboratory, Affiliated Hospital of Putian University, Putian University, Putian, Fujian 351100, China
[2]Guangdong Academy of Sciences, Guangdong-Hong Kong Joint Laboratory of Modern Surface Engineering Technology, Guangdong Provincial Key Laboratory of Modern Surface Engineering Technology, Guangzhou, Guangdong 510651, China
[3]Pharmaceutical and Medical Technology College, Putian University, Putian, Fujian 351100, China
[4]Department of Orthopaedics, The Affiliated Traditional Chinese Medicine Hospital, Southwest Medical University, Luzhou, Sichuan 646000, China

Received: 12 October 2024 / Accepted: 8 May 2025
Published online: 22 May 2025

References

1. Clague MJ, Urbe S, Komander D. Breaking the chains: deubiquitylating enzyme specificity begets function. Nat Rev Mol Cell Biol. 2019;20(6):338–52.
2. Zhu W, Zheng D, Wang D, Yang L, Zhao C, Huang X. Emerging roles of Ubiquitin-Specific protease 25 in diseases. Front Cell Dev Biol. 2021;9:698751.
3. Liu Y, Ma J, Lu S, He P, Dong W. USP25 promotes hepatocellular carcinoma progression by interacting with TRIM21 via the Wnt/β-catenin signaling pathway. 2023;136(18):2229–42.
4. Zheng Q, Song B, Li G, Cai F, Wu M, Zhao Y et al. USP25 Inhibition ameliorates Alzheimer's pathology through the regulation of APP processing and Aβ generation. J Clin Investig. 2022;132(5).
5. Zhong B, Liu X, Wang X, Chang SH, Liu X, Wang A, et al. Negative regulation of IL-17-mediated signaling and inflammation by the ubiquitin-specific protease USP25. Nat Immunol. 2012;13(11):1110–7.
6. Zhou L, Qin B, Yassine DM, Luo M, Liu X, Wang F, et al. Structure and function of the highly homologous deubiquitinases ubiquitin specific peptidase 25 and 28: insights into their pathophysiological and therapeutic roles. Biochem Pharmacol. 2023;213:115624.
7. Wang H, Meng Q, Ding Y, Xiong M, Zhu M, Yang Y, et al. USP28 and USP25 are downregulated by vismodegib in vitro and in colorectal cancer cell lines. FEBS J. 2021;288(4):1325–42.
8. Gersch M, Wagstaff JL, Toms AV, Graves B, Freund SMV, Komander D. Distinct USP25 and USP28 oligomerization States regulate deubiquitinating activity. Mol Cell. 2019;74(3):436–51. e7.
9. Zhong B, Liu X, Wang X, Liu X, Li H, Darnay BG, et al. Ubiquitin-specific protease 25 regulates TLR4-dependent innate immune responses through deubiquitination of the adaptor protein TRAF3. Sci Signal. 2013;6(275):ra35.
10. Zheng Q, Li G, Wang S, Zhou Y, Liu K, Gao Y et al. Trisomy 21-induced dysregulation of microglial homeostasis in Alzheimer's brains is mediated by USP25. Sci Adv. 2021;7(1).
11. Jung ES, Hong H, Kim C, Mook-Jung I. Acute ER stress regulates amyloid precursor protein processing through ubiquitin-dependent degradation. Sci Rep. 2015;5:8805.
12. Shen J, Fu B, Wu Y, Yang Y, Lin X, Lin H, et al. USP25 expression in peripheral blood mononuclear cells is associated with bone mineral density in women. Front Cell Dev Biol. 2021;9:811611.
13. Deng S, Zhou H, Xiong R, Lu Y, Yan D, Xing T, et al. Over-expression of genes and proteins of ubiquitin specific peptidases (USPs) and proteasome subunits (PSs) in breast cancer tissue observed by the methods of RFDD-PCR and proteomics. Breast Cancer Res Treat. 2007;104(1):21–30.
14. Fujimoto A, Totoki Y, Abe T, Boroevich KA, Hosoda F, Nguyen HH, et al. Whole-genome sequencing of liver cancers identifies etiological influences on mutation patterns and recurrent mutations in chromatin regulators. Nat Genet. 2012;44(7):760–4.
15. Nelson JK, Thin MZ, Evan T, Howell S, Wu M, Almeida B, et al. USP25 promotes pathological HIF-1-driven metabolic reprogramming and is a potential therapeutic target in pancreatic cancer. Nat Commun. 2022;13(1):2070.
16. Wang XM, Yang C, Zhao Y, Xu ZG, Yang W, Wang P, et al. The deubiquitinase USP25 supports colonic inflammation and bacterial infection and promotes colorectal cancer. Nat Cancer. 2020;1(8):811–25.
17. Liu C, Zhao D, Ma W, Guo Y, Wang A, Wang Q, et al. Denitrifying sulfide removal process on high-salinity wastewaters in the presence of Halomonas Sp. Appl Microbiol Biotechnol. 2016;100(3):1421–6.
18. Chen S, Zhou Y, Chen Y, Gu J. Fastp: an ultra-fast all-in-one FASTQ preprocessor. Bioinformatics. 2018;34(17):i884–90.
19. Magoc T, Salzberg SL. FLASH: fast length adjustment of short reads to improve genome assemblies. Bioinformatics. 2011;27(21):2957–63.
20. Callahan BJ, McMurdie PJ, Rosen MJ, Han AW, Johnson AJ, Holmes SP. DADA2: High-resolution sample inference from illumina amplicon data. Nat Methods. 2016;13(7):581–3.
21. Bolyen E, Rideout JR, Dillon MR, Bokulich NA, Abnet CC, Al-Ghalith GA, et al. Reproducible, interactive, scalable and extensible Microbiome data science using QIIME 2. Nat Biotechnol. 2019;37(8):852–7.
22. Douglas GM, Maffei VJ, Zaneveld JR, Yurgel SN, Brown JR, Taylor CM, et al. PICRUSt2 for prediction of metagenome functions. Nat Biotechnol. 2020;38(6):685–8.
23. Ward T, Larson J, Meulemans J, Hillmann B, Lynch J, Sidiropoulos D et al. BugBase predicts organism-level Microbiome phenotypes. BioRxiv. 2017:133462.
24. Schloss PD, Westcott SL, Ryabin T, Hall JR, Hartmann M, Hollister EB, et al. Introducing Mothur: open-source, platform-independent, community-supported software for describing and comparing microbial communities. Appl Environ Microbiol. 2009;75(23):7537–41.
25. Segata N, Izard J, Waldron L, Gevers D, Miropolsky L, Garrett WS, et al. Metagenomic biomarker discovery and explanation. Genome Biol. 2011;12(6):R60.
26. Barberan A, Bates ST, Casamayor EO, Fierer N. Using network analysis to explore co-occurrence patterns in soil microbial communities. ISME J. 2012;6(2):343–51.
27. Li H, Durbin R. Fast and accurate short read alignment with Burrows-Wheeler transform. Bioinformatics. 2009;25(14):1754–60.
28. Li D, Liu CM, Luo R, Sadakane K, Lam TW. MEGAHIT: an ultra-fast single-node solution for large and complex metagenomics assembly via succinct de Bruijn graph. Bioinformatics. 2015;31(10):1674–6.

29. Fu L, Niu B, Zhu Z, Wu S, Li W. CD-HIT: accelerated for clustering the next-generation sequencing data. Bioinformatics. 2012;28(23):3150–2.
30. Li R, Li Y, Kristiansen K, Wang J. SOAP: short oligonucleotide alignment program. Bioinformatics. 2008;24(5):713–4.
31. Buchfink B, Xie C, Huson DH. Fast and sensitive protein alignment using DIAMOND. Nat Methods. 2015;12(1):59–60.
32. Beresford-Jones BS, Forster SC, Stares MD, Notley G, Viciani E, Browne HP, et al. The mouse Gastrointestinal Bacteria catalogue enables translation between the mouse and human gut microbiotas via functional mapping. Cell Host Microbe. 2022;30(1):124–38. e8.
33. Bars-Cortina D, Ramon E, Rius-Sansalvador B, Guinó E, Garcia-Serrano A, Mach N, et al. Comparison between 16S rRNA and shotgun sequencing in colorectal cancer, advanced colorectal lesions, and healthy human gut microbiota. BMC Genomics. 2024;25(1):730.
34. Shah N, Tang H, Doak TG, Ye Y. Comparing bacterial communities inferred from 16S rRNA gene sequencing and shotgun metagenomics. Pac Symp Biocomput. 2011:165–76.
35. Sun S, Jones RB, Fodor AA. Inference-based accuracy of metagenome prediction tools varies across sample types and functional categories. Microbiome. 2020;8(1):46.
36. Matchado MS, Ruhlemann M, Reitmeier S, Kacprowski T, Frost F, Haller D et al. On the limits of 16S rRNA gene-based metagenome prediction and functional profiling. Microb Genom. 2024;10(2).
37. Li S, Ma X, Zhang X, Bai S, Li X, Huang Y, et al. Bisphenol S exposure induces intestinal inflammation via altering gut Microbiome. Food Chem Toxicology: Int J Published Br Industrial Biol Res Association. 2024;190:114830.
38. Prasad S, V PS, Abbas HS, Kotakonda M. Mechanisms of antimicrobial resistance: highlights on current advance methods for detection of drug resistance and current pipeline antitubercular agents. Curr Pharm Biotechnol. 2022;23(15):1824–36.
39. Stower H. Antibiotic tolerance leads to antibiotic resistance. Nat Med. 2020;26(2):163.
40. Leuzzi V, Galosi S. Experimental pharmacology: targeting metabolic pathways. Int Rev Neurobiol. 2023;169:259–315.
41. de Vos WM, Tilg H, Van Hul M, Cani PD. Gut Microbiome and health: mechanistic insights. Gut. 2022;71(5):1020–32.

Publisher's note